Taylor & Francis
Taylor & Francis Group

RESEARCH ARTICLE

A stable GH31 α-glucosidase as a model system for the study of mutations leading to human glycogen storage disease type II

Roberta Iacono[a,b‡] 🆔, Francesca Maria Pia Paragliola[a‡] 🆔, Andrea Strazzulli[a,b,c] 🆔 and Marco Moracci[a,b,c] 🆔

[a]Department of Biology, University of Naples "Federico II", Naples, Italy; [b]NBFC, National Biodiversity Future Center, Palermo, Italy; [c]Task Force on Microbiome Studies, University of Naples "Federico II", Naples, Italy

ABSTRACT

GH31 glycosidases are widespread across organisms, but remarkably, less than 1% of them have been biochemically characterised to date. Among them, human lysosomal acid α-glucosidase (GAA) stands out due to its link to Pompe disease, a rare lysosomal storage disorder caused by its deficiency. This disease results in glycogen accumulation, severe cellular damage, motor impairment, and premature death. Structural and functional studies of GAA mutants are challenging due to their instability and lack of activity, hindering their expression and purification. The GH31 enzyme MalA from a hyperthermophilic archaeon is explored here as a stable homolog of GAA. MalA is highly expressible, easy to purify, and structurally characterised. The R400H mutant in MalA, corresponding to the pathogenic GAA R600H mutation, revealed here a 1200-fold drop in specificity constant and >8 °C reduction in thermal stability. We propose MalA's as a robust model for studying GAA mutations and developing therapeutic chaperones.

Introduction

Pompe disease (PD) results from a deficiency in lysosomal acid α-glucosidase (GAA), the enzyme responsible for glycogen breakdown into glucose within the lysosomal lumen. The HGMD database (http://www.hgmd.cf.ac.uk/ac/) lists 656 mutations spread across the entire gene. Clinically, PD presents in varying severities: the severe, often fatal infantile-onset form (IOPD) with less than 1% residual GAA activity, and the milder late-onset forms (LOPD) with up to 20% of normal GAA activity. Current pharmacological treatment of PD is the enzyme replacement therapy (ERT), involving systemic intravenous infusions of Myozyme® recombinant human GAA[1,2], which still present several disadvantages[3–7]. Thus, more studies are needed to understand the molecular bases of the deficient action of GAA mutants through structural and functional approaches that can possibly lead to alternative pharmaceutical approaches.

Recently, the structure of recombinant human GAA was determined by X-ray crystallography using Myozyme® as protein source. The N-terminal β-sheet domain delineates the active site, where conserved residues R600 and D282 play a key role in substrate recognition and stabilisation, while D518 and D616 are essential for catalysis. The c.1799G > A mutation results in the substitution of R600 with a histidine (R600H), a variant commonly found among patients in North America and the Middle East, associated with the IOPD phenotype[3].

So far, functional analyses of GAA mutants have been limited to cell-based assays, conducted either on patient-derived fibroblasts or on GAA mutants transiently expressed in COS-7 cells[8–11]. The scarcity of experimental studies on pure mutant enzymes reflects the technical difficulties due to the intrinsic instability of misfolded proteins and their tendency to aggregate.

Although there are numerous sophisticated in silico prediction tools[12–21], they cannot be used alone to classify a variant nor to define diagnostic parameters by themselves. Therefore, these approaches cannot replace functional analysis[22].

To overcome these limitations, we used the GAA from the hyperthermophilic archaeon Saccharolobus solfataricus 98/2 (MalA)[23,24], as an enzymatic model system of GAA. Both GAA and MalA belong to the large family GH31 of the carbohydrate-active enzyme classification (www.cazy.org)[25]. To date, GH31 family displays more than 30 000 members, 20 subfamilies[26], and exhibits 17 different activities[27]. Among GH31 members, MalA is the only stable homolog of GAA that has been structurally characterised. MalA's intrinsic stability balances the mutation-induced instability, enabling functional studies directly on the mutant enzyme. Although the whole identity of the amino acidic sequence of two enzymes is rather low (about 27%), GAA and MalA belong to the same subfamily 1 and many residues whose mutation leads to PD are conserved.

In this study, MalA serves as the most robust and accessible model system currently available for studying GAA mutants,

enabling the assessment of the effects of individual mutations, analogous to those implicated in the development of PD, on purified mutant enzymes in vitro. This approach could provide valuable insights into whether the observed effects of a mutation primarily impact enzymatic activity or structural stability.

Results and discussion

A new model system of human acid α-glucosidase

Several point mutations on the *gaa* gene encoding the human lysosomal acid GAA, lead to a defective enzyme responsible for PD. The intrinsic instability or the inactivity of the mutants prevent the possibility to study these enzymes in recombinant form, thereby not allowing the identification of the molecular reasons that lead to the disease and to correlate its severity to specific structural and functional changes introduced by the mutations. The search for an enzymatic model system stable enough to perform functional studies prompted us to test another member of family GH31, the GAA from the hyperthermophilic Archaeon *Saccharolobus solfataricus 98/2* (MalA). The whole amino acidic sequence identity between GAA and MalA is 27%. Specifically, the region encompassing the active site amino acids exhibits a higher sequence identity (32% identity from residues 90 to 279) and

Table 1. Pathogenic and likely pathogenic residues in GAA and their corresponding conserved residues in MalA.

GAA residue	MalA residue	Classification
G219	G42	Pathogenic/likely pathogenic
E262	E69	Pathogenic
D282	D87	Pathogenic/likely pathogenic
L291	L98	Pathogenic
Y292	Y99	Pathogenic/likely pathogenic
G359	G167	Pathogenic
P361	P169	Pathogenic/likely pathogenic
W367	W175	Likely pathogenic
R375	R183	Likely pathogenic
D404	D203	Pathogenic
Y407	Y215	Likely pathogenic
M408	M216	Likely pathogenic
Y455	Y260	Pathogenic
P457	P262	Pathogenic/likely pathogenic
F467	K270	Likely pathogenic
G478	G281	Pathogenic/likely pathogenic
W481	W284	Pathogenic
P482	P285	Likely pathogenic
D489	D292	Pathogenic/likely pathogenic
D513	D315	Likely pathogenic
M519	M311	Pathogenic
N520	N312	Pathogenic
E521	E323	Pathogenic/likely pathogenic
P522	P324	Pathogenic/likely pathogenic
H568	H368	Pathogenic/likely pathogenic
S599	S399	Pathogenic/likely pathogenic
R600	R400	Pathogenic/likely pathogenic
T614	T414	Pathogenic/likely pathogenic
G615	G415	Pathogenic/likely pathogenic
D616	D416	Pathogenic/likely pathogenic
L632	L432	Pathogenic
G638	G438	Pathogenic/likely pathogenic
V642	V442	Likely pathogenic
G643	G443	Pathogenic/likely pathogenic
D645	D445	Pathogenic/likely pathogenic
R672	R478	Pathogenic/likely pathogenic
R702	R508	Pathogenic/likely pathogenic
V723	V529	Pathogenic/likely pathogenic
R725	R531	Pathogenic/likely pathogenic

Here, the pathogenic residues of GAA that are conserved in MalA at the interface among the monomers have not been included.

significant conservation (50% positives from residues 140 to 279). In addition, GAA is a monomer in solution while MalA is a hexamer, with the RMSD of their superimposed monomers being 1.13 Å (Figure S1). Notably, in MalA, 39 amino acid residues associated with PD, as reported in the NCBI ClinVar database (https://www.ncbi.nlm.nih.gov/clinvar/), are invariant and not involved in the oligomerisation of the enzyme (Table 1, Figure 1(A), Figure S1). These residues are classified as pathogenic or likely pathogenic depending on the substitutions observed in different patients. Furthermore, in the region of the active site, nine amino acids implicated in PD remain invariant between the two enzymes (Figure 1(B,C) and Figure S2).

MalA has been characterised in detail under the kinetical and structural point of view[24,28] and it is the most stable GH31 member characterised so far (as reported on CAZy database – www.cazy.org – December 2024). Moreover, MalA is able to efficiently hydrolyse glycogen, such as GAA, with a specific activity of 1.0 μmol of glucose/min at 85 °C[29].

For these reasons, the production of a mutant in the active site of MalA, corresponding to a pathogenic form of GAA, was undertaken. R600H is one of the five most frequently reported missense mutations associated with infantile-onset Pompe disease (IOPD)[30]. The transiently expressed R600H mutant in COS-7 cells, the only possible approach that can be used today as patients' fibroblast is not available, showed less than 2% of activity compared to GAA wild-type[8]. The R600 residue in GAA corresponds to MalA R400, which we consequently mutated to histidine (R400H) to assess whether it reproduces a similarly severe effect in its hyperthermophilic homolog.

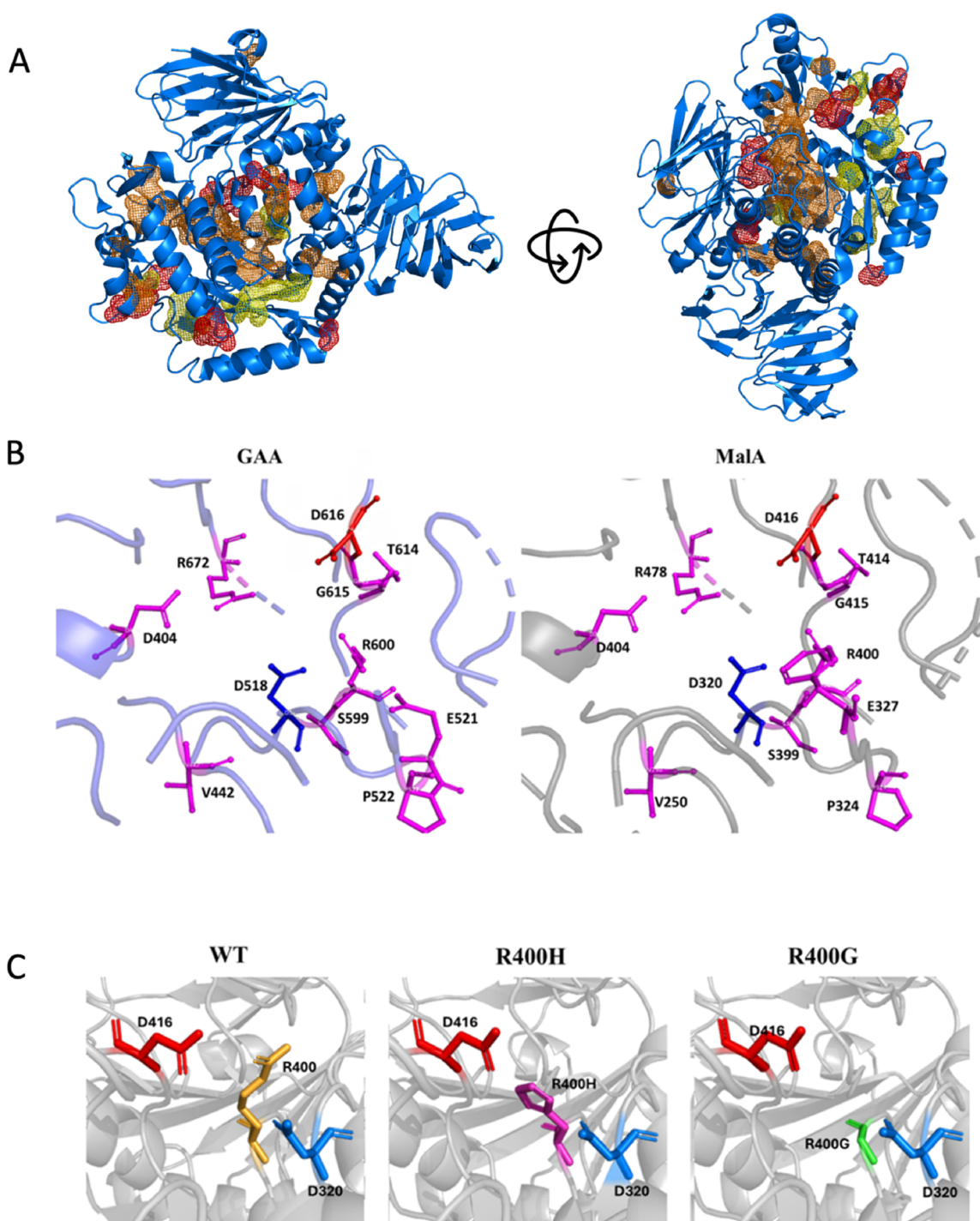### Analysis of the role of R400 in the catalysis of MalA

The crystal structure of MalA superimposed on that of the GH31 α-xylosidase from *Escherichia coli* (YicI – PDB-ID 1XSK) presenting in the −1 position of the active site a 5-fluoro-xylopyranosyl residue (5F-Xyl) covalently bound to the catalytic nucleophile, showed that R400 interacts with the hydroxyl bound to carbon 2 (OH-2)[24]. Instead, in the 3D-structure of MalA, in which a β-octyl-glucopyranoside (β-O-Glc) is bound in the +1 position of the active site (PDB-ID 2G3N), R400 interacts with OH-3. As a comparison, in GAA, the corresponding R600 interacts with OH-2 of either the inhibitors 1-deoxynojirimycin (1-DNJ) and *N*-hydroxyethyl-DNJ (NHE-DNJ), occupying the −1 substrate binding site, or the OH-3 of the glucose residue of acarbose located in the +1 binding site[31]. Although this evidence suggests that R400 and R600 in MalA and GAA, respectively, are both involved in the ligand binding, the identification of their conclusive role is still elusive, considering that it formed interactions when ligands occupy the interface between the −1 and +1 subsites. To investigate more in depth the role of R400 residue in the active site of MalA, a second mutant, R400G, was produced, in which the side chain was completely removed.

To evaluate the effect of the mutations of R400 in both His and Gly on the activity of MalA, the steady-state kinetic constants on the substrates para-nitrophenyl-α-D-glucopyranoside (pNP-α-D-Glc), 4-methylumbelliferyl-α-D-glucopyranoside (MU-α-D-Glc), and maltose were measured (Table 2). In both mutants, the affinity to the three substrates does not significantly change with the corresponding K_M values of the same order of magnitude of the wild type. Instead, the two mutants show a remarkable decrease in their activity with a turnover number drastically reduced on all substrates tested (~100-fold on pNP-α-D-Glc and maltose and >700-fold on MU-α-D-Glc), confirming that R400 plays a significant

Figure 1. Structural comparison between the human acidic α-glucosidase (GAA) and the α-glucosidase from *Saccharolobus solfataricus* (MalA). (A) Pathogenic and likely pathogenic residues mapped on the MalA monomer. The figure shows 39 residues linked to Pompe disease mapped on the MalA monomer. Colours indicate their classification: pathogenic (red), pathogenic/likely pathogenic (orange), and likely pathogenic (yellow). (B) Close-up view (8 Å) of the active sites of MalA (PDB ID 2G3M, blue backbone, left panel) and GAA (PDB ID 5KZW grey backbone, right panel). Both the catalytic nucleophile and acid/base residues are highlighted in blue (D320/D518 as the nucleophile and in red D416/D616 as the acid/base in MalA and GAA, respectively). Conserved residues between MalA and GAA's active sites, associated with Pompe disease mutations, are highlighted in magenta; (C) structural prediction of the MalA active site mutations.

role in MalA catalysis. These results are in agreement with the activity data obtained in COS-7 cells transfected with the mutant expressing GAA wild-type and the R600H mutant in which the latter maintain only less than 2% of activity of the wild type on the substrate MU-α-D-Glc[8]. However, COS-7 cells transfected did not allow verifying if the lack of activity is the result of a weaker substrate binding or reduced turnover number, that is instead demonstrated in MalA R400H.

Analysis of the role of R400 residue in the thermostability of MalA

Thermostability is a parameter that indicates a protein's resistance to thermal denaturation and can be used as an indirect indicator of its conformational state and ability to maintain its native structure. In this context, the thermostability of MalA and its mutants was evaluated to quantify the impact of the mutation R400 on

protein structure, particularly considering the known instability of mutant GAA enzymes. To assess whether R400 is effectively involved in the thermostability of MalA, the melting temperature (T_m) was evaluated by using the differential scanning fluorimetry (DSF) approach for both wild-type and mutants (Figure 2).

The T_m of the wild-type and of both mutants R400H and R400G at pH 8.0 is 77.0 ± 1.7 °C, 64.2 ± 0.2 °C, and 65 ± 0.2 °C, respectively, indicating that, at these conditions, the substitution of R400 destabilises MalA of about 13 °C, even if a positive charge was present in the mutant R400H. Instead, at both pH 5.0 and 7.0, MalA WT and mutants are so resistant to thermal denaturation that it was not possible to measure the T_m (data not shown). This likely reflects the high stability of both the wild-type and mutants at these pH values, which exceeds the detection limit of the thermal ramp used (see "Materials and methods" section).

Functional thermostability was also evaluated by incubating the enzymes at 65 °C and 85 °C, with residual activity measured at regular intervals under standard conditions. At 65 °C, MalA wild-type retains 56% activity after 6 h. Conversely, at 85 °C, the residual activity was 44% after 10 min of incubation. Also, the MalA R400G mutant was susceptible to incubation at the tested temperatures. It exhibits a 40% residual activity after 10 min at 85 °C, while the R400H mutant became completely inactive after 10 min at the same temperature, indicating poor stability at elevated temperatures (data not shown). A clear correlation was observed between decreased thermostability (especially for the R400H mutant) and the loss of catalytic activity, suggesting that

residue R400 in MalA is involved in both the enzyme's activity and stability. It is worth mentioning that the T_m values of recombinant GAA at pH 7.4 and 4.0 are 47.9 ± 0.7 and 53.7 ± 0.2, respectively (Figure S3), which are 29.1 °C and 23.3 °C less than MalA WT at pH 8.5, as expected from the comparison between a mesostable and thermostable enzyme. Nevertheless, it is worth noting that both enzymes show higher stability at acidic pH, confirming that MalA could be a good model system of GAA. Again, the availability only of data of GAA R600H mutant expressed in COS cells, but not purified, precluded any measurement of structural and functional stability. However, our data, for the first time strongly suggest that the R600H mutant dramatically affects not only the GAA activity, but also its stability, explaining significant impairments associated with its IOPD phenotype.

Effect of competitor inhibitors used as pharmacological chaperones on MalA wild-type and R400 mutants

Recently, complementary therapeutic strategy to ERT has been approved for the treatment of adults with late-onset Pompe disease (LOPD)[32]. On March 2023, Amicus Therapeutics (Philadelphia, PA) received the first approval in the EU for cipaglucosidase alfa (Pombiliti™), that is a recombinant human acid GAA along with the enzyme stabiliser miglustat (NB-DNJ) as a two-component therapy combining ERT and pharmacological chaperone therapy (PCT). Briefly, the approach of PCT is based on the concept that small molecules, often competitive inhibitors, enhance the stability and function of misfolded enzymes, potentially offering significant clinical benefits[11,33–35]. These molecules influence key processes including protein synthesis, folding, trafficking, aggregation, and degradation. So far, the effects of chaperone therapy on mutated GAA have been studied in fibroblasts and HeK cells derived from IOPD and LOPD patients[33] and COS-7 cells transfected with different GAA mutant gene, including R600H[8]. The chaperone effect of 1-DNJ on this variant has been observed by analysing the GAA activity on MU-α-D-Glc substrate levels of mature GAA species[8]. Again, the intrinsic instability of mutants leading to IOPD and LOPD phenotypes precluded detailed studies on the chaperoning effect of small ligands on pure human GAA.

The steady-state kinetic constants and stability parameters were measured to understand the behaviour of MalA mutants in the presence of three well-known inhibitors of GAA, namely 1-DNJ,

Table 2. Kinetic constants of the three enzymes with, in order: pNP-α-D-Glc, MU-α-D-Glc, and maltose at 85 °C, pH 5.0.

Enzyme	K_M (mM)	k_{cat} (s^{-1})	k_{cat}/K_M (s^{-1}·mM^{-1})
	pNP-α-D-Glc		
MalA wild-type	0.8 ± 0.001	113.4 ± 0.004	141.8
R400H	0.26 ± 0.03	1.1 ± 0.03	4.2
R400G	0.12 ± 0.01	0.5 ± 0.006	4.2
	MU-α-D-Glc		
MalA wild-type	4.04 ± 0.04	1275 ± 0.01	315.6
R400H	7 ± 0.02	1.8 ± 0.212	0.26
R400G	4.25 ± 0.05	1.1 ± 0.2	0.26
	Maltose		
MalA wild-type	4.4 ± 0.002	786 ± 0.005	178.6
R400H	4.2 ± 0.04	5.1 ± 0.4	1.22
R400G	3.9 ± 0.04	2.7 ± 0.1	0.7
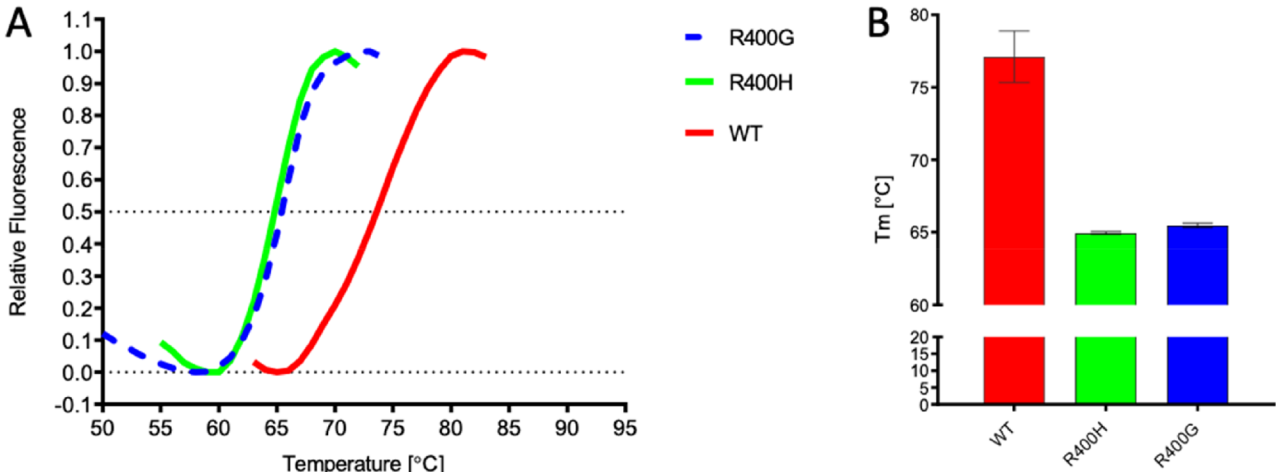
Figure 2. Analysis of the stability of wild-type and mutants by DSF. (A) Thermal scan profile and (B) melting temperature of MalA wild-type and their mutants.

Table 3. Values of IC$_{50}$ for each enzyme (WT, R400G, R400H) with the inhibitors 1-DNJ, acarbose, and NB-DNJ.

Inhibitor	WT	R400H	R400G
	IC$_{50}$ (µM)		
1-DNJ	0.1 ± 0.01	30 ± 2.3	224.3 ± 41
NB-DNJ	1.7 ± 0.2	5.7 ± 0.21	55 ± 6.62
Acarbose	20.2 ± 0.9	830 ± 91.5	912.2 ± 67.5

Table 4. Values of K_i for each enzyme (WT, R400G, R400H) with the inhibitors 1-DNJ, acarbose, and NB-DNJ.

Inhibitor	WT	R400H	R400G
	K_i (µM)		
1-DNJ	0.009	2.2	1.4
NB-DNJ	0.13	0.7	0.13
Acarbose	0.98	72	23

Table 5. Analysis of the stability by differential scanning fluorimetry in presence of 1-deoxynojirimycin, acarbose, and *N*-butyldeoxynojirimycin inhibitors on wild-type and mutants.

	T_m MalA WT	ΔT_m
No inhibitor	77.0 ± 1.0	
0.1 mM 1-DNJ	84.1 ± 0.5	+7.0
0.8 mM 1-DNJ	87.1 ± 0.3	+10.1
0.1 mM NB-DNJ	86 ± 0.7	+8.9
0.8 mM NB-DNJ	85.1 ± 0.6	+8.0
0.4 mM acarbose	79.1 ± 0.9	+2.0
1.0 mM acarbose	79.8 ± 0.7	+2.8
	T_m MalA R400H	ΔT_m
No inhibitor	64.2 ± 0.2	
0.1 mM 1-DNJ	65.5 ± 0.2	+1.3
0.8 mM 1-DNJ	64.1 ± 0.1	0
0.1 mM NB-DNJ	64.7 ± 0.4	+0.5
0.8 mM NB-DNJ	61.7 ± 0.1	−2.4
0.4 mM acarbose	64.2 ± 0.1	0
1.0 mM acarbose	64.2 ± 0.2	+0.1
	T_m MalA R400G	ΔT_m
No inhibitor	65.0 ± 0.02	
0.1 mM 1-DNJ	66.4 ± 0.2	+1.5
0.8 mM 1-DNJ	67.5 ± 0.3	+2.5
0.1 mM NB-DNJ	65.6 ± 0.2	+0.6
0.8 mM NB-DNJ	63.5 ± 0.1	−1.5
0.4 mM acarbose	65 ± 0.04	0
1.0 mM acarbose	65 ± 0.1	0

N-butyldeoxynojirimycin (Miglustat, NB-DNJ), and acarbose[36] (Figure S4).

The IC$_{50}$ values of the wild-type and mutants in relation to the three inhibitors were assessed (see Table 3 and Figure S5). IC$_{50}$ values of MalA with 1-DNJ and NB-DNJ are two orders of magnitude lower, compared to the IC$_{50}$ values obtained from recombinant GAA, 20 µM and 158 µM, respectively[9,34].

Instead, the two mutants exhibit more significant inhibition at higher concentrations than MalA wild-type for all inhibitors. In particular, R400H showed an IC$_{50}$ value that exceeds that of the wild-type by more than two orders of magnitude for 1-DNJ. Of particular note is R400G, which has an IC$_{50}$ value that is one and three orders of magnitude higher than that of R400H and of the wild type, respectively, suggesting the substitution of R400 reduces the inhibitory effect of the 1-DNJ.

The wild type has a two orders of magnitude higher IC$_{50}$ on the pseudo-tetrasaccharide acarbose (20.2 ± 0.9 µM), if compared to 1-DNJ (0.1 ± 0.01 µM), highlighting a stronger inhibitory effect of an analogue of the reaction product rather than an analogue of a malto-oligosaccharide substrate.

On the other deoxynojirimycin derivative, NB-DNJ, MalA wild-type has an IC$_{50}$ value 1 order of magnitude higher than 1-DNJ. Interestingly, both mutants exhibit an IC$_{50}$ that is of the same order of magnitude than the wild type (R400H) or only one order of magnitude higher (R400G), indicating that the *N*-butyl chain in NB-DNJ reduced the affinity of the molecule in the active site of the MalA (Table 3). Unlike 1-DNJ, the IC$_{50}$ values for acarbose are more than 40-fold higher in the R400H and -G mutants than the wild type, and they were rather similar to each other, suggesting that for these kinds of mutations substrate-mimicking inhibitors have similar effects.

To determine the inhibition constants for MalA wild-type and R400 mutants, inhibition kinetics with 1-DNJ, acarbose, and *N*-butyldeoxynojirimycin were performed for each enzyme. 1-DNJ is the strongest inhibitor of the wild type; conversely, the two mutants showed the lowest K_i with NB-DNJ, as reported in Table 4.

Interestingly, NB-DNJ has a similar inhibitory effect to 1-DNJ on MalA WT but is stronger with the two mutants than 1-DNJ. Indeed, MalA wild-type and the R400G mutant have the same K_i value, while the mutant in His shows a K_i just 5.4-fold higher than WT, indicating that the mutations weakly affect the inhibitory effect of NB-DNJ. This suggests the *N*-butyl group might induce conformational changes in MalA structure by forming new stabilising interactions with the surrounding amino acids. For instance, in recombinant GAA, the surroundings of the active site revealed a

high degree of plasticity, as the binding of NHE-DNJ induces remarkable conformational changes to the side chains of M519 and W481 leading to the formation of a hydrogen bond with the latter aminoacid[31]. So, in MalA, the putative conformation induced by NB-DNJ could balance the substitution of Arg in His or Gly, thanks to the formation of new stabilising interactions.

On acarbose, the three enzymes showed the lowest inhibitory effect in agreement with the IC$_{50}$ data. The K_i of acarbose for the MalA wild-type (0.98 µM) is 10 times higher than that of 1-DNJ, indicating a weaker inhibitory effect compared to the iminosugar. Both R400H and R400G mutants exhibit significantly higher K_i values than the wild type, with R400H showing even greater K_i values than R400G, indicating that the imidazole ring reduces inhibitor affinity more than the loss of the arginine side chain.

Analysis of thermal stabilisation in MalA mutants via pharmacological chaperones

The resistance of wild-type enzymes to physical stresses, such as changes in temperature and pH, is commonly used as an indicator to assess the effectiveness of pharmacological chaperones[9,11,33]. An increase in thermostability induced by chaperone addition can thus be interpreted as improving protein structure and resilience to stress[9–11,31].

In this regard, DSF was performed in the presence of 1-DNJ, NB-DNJ, and acarbose to study their possible stabilising effect on the two MalA mutants (Table 5 and Figure S6). The concentration of inhibitors was carefully chosen to be at least two orders of magnitude higher than their respective K_i, ensuring a robust analysis of their stabilising effects on the thermally unstable MalA mutants.

The DSF analysis revealed that the wild-type incubated with deoxynojirimycin derivatives showed ΔT_m increase in the range +7–10 °C, similarly to recombinant GAA showing an increment of 12 °C[11]. For the R400H and -G mutants, the stabilising effect of 1-DNJ and NB-DNJ is much less evident ranging from +0.5 °C

(0.1 mM NB-DNJ on R400H) to +2.5 °C (0.8 mM 1-DNJ on R400G), with cases where the presence of the ligand had no or slightly destabilising effect (0 °C and −2.5 °C on R400H mutant in 0.8 mM 1-DNJ and NB-DNJ, respectively). Acarbose stabilised MalA wild-type by ~2.0 °C, while no effect on the mutants has been observed. These data confirm that kinetic parameters cannot be easily used to predict the stabilising effect on the proteins[37] and that the inhibitors interact differently with a catalytic site, which has acquired an altered architecture by mutagenesis.

To evaluate the possible stabilising effect of allosteric chaperones on the R400 mutations in MalA, N-acetylcysteine (NAC) (Figure S4), which has been proven to bind distantly from the active site of GAA with no inhibitory effect[31], was assayed. This compound, which increased the T_m by 10.5 ± 0.5 °C at 10 mM concentration, is a specific chaperone of GAA, while no stabilising effect on another GH31 GAA from rice has been observed[9,31] (Figure S7). Scanning fluorescence in the absence and presence of 30 mM NAC revealed that the wild-type and R400G enzymes exhibit increased stability up to ~2.5 °C in 30 mM NAC. Instead, R400H mutant shows a ΔT_m of +3.5 °C if compared to the control (Table 6, Figure S8). Indeed, as observed in the superimposition of the three-dimensional structures of MalA and GAA, one of the two NAC binding pockets, specifically the low-affinity site, is structurally conserved, suggesting a common mechanism of binding (Figure 3)[31]. Possibly, the inherent thermal stability of MalA relative to recombinant GAA, may account for why NAC stabilised MalA

wild-type at a lower extent than GAA (3.5 °C vs. 10.5 °C, respectively) and at 30 mM, rather than at 10 mM concentration. In addition, the different oligomeric structure of MalA (examer) if compared to NAC (monomer) could also play a role in the stabilising mechanisms of the PC. Although NAC is a pharmacological chaperone on MalA not as efficient as on GAA, it is worth noting that NAC, a PC not binding to the active site, is able to stabilise the mutation R400H whose homologue in humans is responsible of a IOPD phenotype (see Table 5). The inactivation of the mutant produced by the change of Arg into His, might have affected also the binding of the competitive inhibitors, thereby reducing their chaperoning efficiency. Instead, the mutation might have left the binding site for allosteric chaperones, such as NAC, unaffected. This would explain why NAC can still promote a chaperoning effect on the mutant, although at high concentrations.

Our results offer for the first time the possibility of analysing the effect of pathological mutations in PD in vitro on a possible model system of GAA and to test the effect of pharmacological chaperones on a mutant responsible of a IOPD phenotype. This study highlights the importance of assessing the efficacy of pharmacological chaperones for each specific enzyme mutation, as different mutations can affect binding and stabilisation in diverse ways.

Conclusions

This study proposed the thermostable GAA MalA from S. solfataricus 98/2 as a model system to investigate the effects of the R600H mutation, associated with PD, on the human enzyme GAA. Although MalA and GAA share low amino acid sequence identity, they exhibit high structural similarity at the active site. In addition, MalA is the only stable homolog of GAA that has been structurally characterised. To test the validity of the model, we have chosen a residue in GAA (R600) producing a severe reduction of the enzyme, so that we can see if MalA would be able to sustain such modification. The R400H mutant in MalA, corresponding to the R600H mutation in GAA, could be expressed and purified although showing a drastic reduction in enzymatic activity and thermal stability, supporting the observation that the R600H mutation significantly impairs GAA activity. Additionally, among competitive inhibitors commonly used in PCT for GAA, only 1-DNJ slightly stabilised the R400H and R400G mutants. Instead, the compound NB-DNJ showed a strong inhibition on the mutants without any stabilising

Table 6. Analysis of the stability by differential scanning fluorimetry in the presence of N-acetylcysteine (NAC) on WT and mutants.

	T_m MalA WT	ΔT_m
CTL	77.0 ± 1.0	
10 mM NAC	75.8 ± 0.86	−1.2
30 mM NAC	79.6 ± 0.54	+2.6
	T_m MalA R400H	ΔT_m
CTL	64.2 ± 0.03	
10 mM NAC	64.9 ± 0.03	+0.7
30 mM NAC	67.7 ± 0.13	+3.5
	T_m MalA R400G	ΔT_m
CTL	65 ± 0.15	
10 mM NAC	65.5 ± 0.04	+0.5
30 mM NAC	67.3 ± 0.11	+2.3

CTL: control.
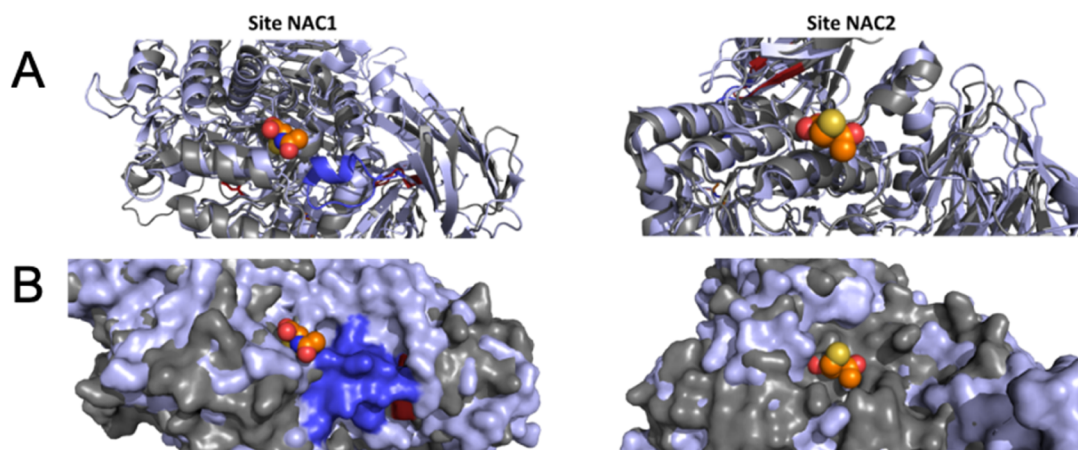
Figure 3. Comparison of the N-acetyl cysteine binding sites of human GAA (light blue) and MalA WT (grey). The functional and surface representation is shown in (A) and (B), respectively. Detail of the full affinity site (NAC1) and low-affinity site (NAC2) for NAC.

effects observed. Interestingly, the allosteric chaperone NAC exhibited a more significant stabilising effect, resulting in an increase in stability of approximately 2.5 °C for both the wild-type and R400G, and a ΔT_m of +3.5 °C for R400H at a concentration of 30 mM NAC. Although it is essential to recognise that thermostability does not fully capture all factors affecting enzyme stability *in vivo* (cellular environment, interactions with other biomolecules, enzyme turnover mechanisms), this approach provides valuable information on the activity and stability of the mutants and the effect of pharmacological chaperones.

This result emphasises the importance of evaluating the effect of each specific enzyme mutation, that can variably influence activity and/or stability as well as binding and stabilisation by using pharmacological chaperones. The use of MalA mutants as a model is particularly advantageous due to their capacity for recombinant expression, supported by the inherent robustness of this hyperthermostable enzyme. This feature is not achievable with GAA mutants, whose instability precludes successful recombinant expression. This approach offers a practical alternative for probing the effects of specific mutations and potential therapeutic interventions in systems where direct study of the human enzyme is challenging.

Materials and methods

Materials

All commercially available substrates were purchased from Sigma-Aldrich (St. Louis, MO), Carbosynth (Shrewsbury, UK), and Megazyme (Bray, Ireland).

The synthetic genes pET29b(+)_MalA *Wild Type*, pET29b(+)_MalA *R400G*, and pET29b(+)_MalA *R400H* were provided by NZYtech (Lisbon, Portugal), the gene is under the control of an isopropyl-1-thio-β-D-galactopyranoside (IPTG) inducible T7 RNA polymerase promoter and the C-terminal of the protein was fused to 6xHis tag. Each sequence was optimised using the codon usage of *E. coli*.

The commercial inhibitors 1-DNJ and acarbose were purchased from Sigma-Aldrich (St. Louis, MO) while *N*-butyldeoxynojirimycin (hydrochloride) from Cayman Chemical (Ann Arbor, MI).

In silico analysis

The amino acid sequence alignment was carried out using Clustal Omega[38] with the FASTA sequences available on GenBank: AC38215.1 (alpha-glucosidase MalA, *Saccharolobus solfataricus* 98/2) and CAA68763.1 (GAA, *Homo sapiens*).

The structure superimposition was performed with PyMol (Schrödinger and DeLano, 2020. PyMOL. Retrieved from http://www.pymol.org/pymol) using the available structures (PDB-ID: 2G3M and 5NN3)[24,31].

Expression and purification

The three sequences were expressed in *Escherichia coli* cells, strain BL21 (DE3) RIL. The cells transformed with pET29b(+)_MalA *Wild-type/R400G/R400H* were grown at 37 °C in Luria–Bertani (LB) broth supplemented with Kanamycin (50 μg mL^{-1}) and chloramphenicol (34 μg mL^{-1}). Gene expression was induced by the addition of 1 mM IPTG when the culture reached an A_{600} of 0.6. Growth was allowed to proceed for 16 h, and cells were harvested by centrifugation at 6000 × g. The resulting cell pellet was resuspended in 20 mM sodium phosphate buffer, pH 7.3, 150 mM NaCl, and 1% TRITON-X100 with a ratio of 4 mL g^{-1} cells and then was incubated for 1 h with 20 mg of lysozyme (Fluka, Buchs, Switzerland) and 5 mg DNase I (Neofroxx, Einhausen, Germany). Cells were lysed by freeze and thaw and cell debris was removed by centrifugation at 17 000 × g for 30 min. The free cellular extract (FCE) was heat-fractionated for 15 min at 70 °C and after centrifugated. The heat-fractioned samples were loaded on a HisTrap HP 1 mL (GE Healthcare, Chicago, IL) equilibrated with 50 mM sodium phosphate buffer, pH 7.5, and 150 mM NaCl (buffer A). The protein was eluted with a two-step gradient of imidazole in buffer A (250 mM imidazole, 10-column volumes followed by 500 mM imidazole, 10-column volumes) at a flow rate of 1 mL min^{-1}. The protein was eluted at 250 mM imidazole. The active fractions were pooled and dialysed against 20 mM sodium phosphate buffer, pH 7.3, and 150 mM NaCl (PBS buffer). The enzymes were stored at 4 °C. The protein concentration was determined using the method of Bradford[39] by using bovine serum albumin as standard.

Characterisation of MalA wild-type and relative mutants

The standard assay for MalA wild-type and its mutants was performed on 10 mM pNP-α-D-Glc in 100 mM sodium citrate buffer at pH 5.0 at 85 °C by using 0.9 μg of MalA wild type, 26 μg of MalA R400H, and 45 μg of MalA R400G in a final volume of 200 μL. After 2 min of incubation, the reaction was blocked in ice and by adding 800 μL of 1 m sodium carbonate pH 10.2. The absorbance was spectrophotometrically measured at 420 nm at room temperature using a Cary 1E (Addison, IL). The kinetics studies on pNP-α-D-Glc were carried out in presence of 0.05–20 mM of substrate. Whereas the activity on maltose was carried out in standard condition in presence of 0.1–20 mM substrate, using 1.5 μg of MalA wild type, 41.6 μg of MalA R400H, and 62.3 μg of MalA R400G determined by measuring the released glucose with the glucose oxidase-peroxidase enzymatic assay (GOPOD), considering that one molecule of maltose leads to the release of two glucose units. One unit of enzyme activity was conventionally defined as the amount of enzyme which hydrolyses 1.0 μmol of the substrate in 1.0 min under standard conditions.

The kinetic studies on fluorescent substrate MU-α-D-Glc using 0.04 μg of MalA wild type, 0.132 μg of MalA R400H, and 0.4 μg of MalA R400G were performed in standard condition using the range of substrate 5 μM to 5 mM. The activity was monitored and quantified by measuring the fluorescence of methylumbelliferone at λ_{ex} 360 nm and λ_{em} 450 nm, using an FP-8600 fluorescence spectrometer (Jasco, Hachioji, Japan).

pH and temperature dependence

The temperature dependence of the activity of the enzyme in this study was determined in the range 30–95 °C in 100 mM sodium citrate buffer (pH 5.0) with 10 mM pNP-α-D-Glc as substrate.

Optimal pH was determined by assaying the enzymes with 10 mM pNP-α-D-Glc at 85 °C for 2 min in 100 mM of sodium citrate buffer (pHs 3.0–5.5), 100 mM sodium phosphate buffer (pHs 6.0–8.0), and 100 mM sodium borate (pHs 8.0–10).

Inhibition studies

Inhibition studies were conducted under the standard conditions described above on 10 mM pNP-α-D-Glc.

The IC_{50} value of the three enzymes was measured by using increasing concentrations of the different inhibitors: 1-DNJ up to

5 mM, acarbose up to 9 mM and *N*-butyldeoxynojirimycin (NB-DNJ) up to 1 mM.

Inhibition kinetics with 1-DNJ, acarbose and *N*-butyldeoxynojirimycin were performed for each enzyme at 85 °C, as described above by using [1-DNJ] between 0.02 μM and 25.0 μM, [acarbose] between 10.0 and 500 μM, and [NB-DNJ] between 0.5 and 25.0 μM.

Studies of thermal stability

Functional thermostability was assessed by incubating the enzymes in optimum condition at 65 and 85 °C for up to 24 h. The residual activity was measured in triplicate after 10 min, 30 min, 1 h, 2 h, 3 h, 4 h, 6 h, and 24 h, following the standard assay previously reported.

The structural stability of MalA and its mutants was evaluated. Each enzyme (1.4 mg) was mixed with 0.2 M sodium citrate buffer pH 5.0, sodium phosphate buffer pH 7.0, or sodium-borate buffer at pH 8.5. SYPRO™ Orange Protein Gel Stain 5X (Invitrogen, Thermo Fisher Scientific, Waltham, MA) was added. The mixtures (50 μL) were prepared in triplicate and loaded into a sealed, clear white 96-well PCR plate. The assay was conducted using the StepOnePlus Real-Time PCR System (Applied Biosystems, Thermo Fisher Scientific, Waltham, MA). Samples were initially incubated at 25 °C for 10 min, followed by a thermal scan from 25 °C to 95 °C with 1 °C increments every 10 min. After reaching 95 °C, samples were incubated for an additional 10 min, as described previously. The structural stability of recombinant GAA (2.5 μg) was measured in 150 mM NaCl, 50 mM buffer sodium phosphate pH 7.4 or buffer sodium acetate at pH 4.5, in the presence of SYPRO™ Orange Protein Gel Stain 5X (Invitrogen, Thermo Fisher Scientific, Waltham, MA). The mixtures were prepared in triplicate. The thermal scan from 25 °C to 95 °C with 1 °C increments every 1 min. The structural stability of GAA from rice type V (2.5 μg) (Sigma-Aldrich, St. Louis, MO) was measured in 0.2 M buffer sodium borate pH 8.0 in the presence of SYPRO™ Orange Protein Gel Stain 5X (Invitrogen, Thermo Fisher Scientific, Waltham, MA). The mixtures were prepared in triplicate. The thermal scan from 25 °C to 95 °C with 1 °C increments every 0.5 min. Protein unfolding was monitored by tracking changes in SYPRO™ Orange fluorescence, which was normalised to the maximum fluorescence in each scan to derive relative values. Melting temperatures were calculated according to Niesen et al.[40] For the determination of the melting temperature, experimental data were best fitted using the software GraphPad Prism (GraphPad Software, San Diego, CA). The standard deviations for each melting temperature were calculated from six replicates. Moreover, thermal stability scans of MalA and the mutant were carried out, as previously shown, in the presence of 0.1 and 0.8 mM 1-DNJ, 0.4 and 1.0 mM acarbose, 0.1 and 0.8 mM NB-DNJ and then 10 and 30 mM NAC.

Acknowledgements

Author contributions

Disclosure statement

Funding

ORCID

Roberta Iacono 🔬 http://orcid.org/0000-0002-3586-4322
Francesca Maria Pia Paragliola 🔬 http://orcid.org/0000-0002-9254-5651
Andrea Strazzulli 🔬 http://orcid.org/0000-0002-9690-149X
Marco Moracci 🔬 http://orcid.org/0000-0002-9846-2531

Data availability statement

The authors confirm that the data supporting the findings of this study are available within the article [and/or] its supplementary materials.

References

1. van der Ploeg AT, Reuser AJ. Pompe's disease. Lancet. 2008;372(9646):1342–1353.
2. Montagnese F, Barca E, Musumeci O, Mondello S, Migliorato A, Ciranni A, Rodolico C, De Filippi P, Danesino C, Toscano A. Clinical and molecular aspects of 30 patients with late-onset Pompe disease (LOPD): unusual features and response to treatment. J Neurol. 2015;262(4):968–978.
3. Dornelles AD, Junges APP, Pereira TV, Krug BC, Gonçalves CBT, Llerena JC, Kishnani PS, de Oliveira HA, Schwartz IVD. A systematic review and meta-analysis of enzyme replacement therapy in late-onset Pompe disease. J Clin Med. 2021;10(21):4828.
4. de Vries JM, Kuperus E, Hoogeveen-Westerveld M, Kroos MA, Wens SC, Stok M, van der Beek NA, Kruijshaar ME, Rizopoulos D, van Doorn PA, et al. Pompe disease in adulthood: effects of antibody formation on enzyme replacement therapy. Genet Med. 2017;19(1):90–97.
5. Angelini C, Semplicini C, Ravaglia S, Bembi B, Servidei S, Pegoraro E, Moggio M, Filosto M, Sette E, Crescimanno G, et al. Observational clinical study in juvenile-adult glycogenosis type 2 patients undergoing enzyme replacement therapy for up to 4 years. J Neurol. 2012;259(5):952–958.
6. Strothotte S, Strigl-Pill N, Grunert B, Kornblum C, Eger K, Wessig C, Deschauer M, Breunig F, Glocker FX, Vielhaber S,

et al. Enzyme replacement therapy with alglucosidase alfa in 44 patients with late-onset glycogen storage disease type 2: 12-month results of an observational clinical trial. J Neurol. 2010;257(1):91–97.

7. van der Ploeg A, Carlier PG, Carlier RY, Kissel JT, Schoser B, Wenninger S, Pestronk A, Barohn RJ, Dimachkie MM, Goker-Alpan O, et al. Prospective exploratory muscle biopsy, imaging, and functional assessment in patients with late-onset Pompe disease treated with alglucosidase alfa: the EMBASSY study. Mol Genet Metab. 2016;119(1–2):115–123.

8. Flanagan JJ, Rossi B, Tang K, Wu X, Mascioli K, Donaudy F, Tuzzi MR, Fontana F, Cubellis MV, Porto C, et al. The pharma-cological chaperone 1-deoxynojirimycin increases the activity and lysosomal trafficking of multiple mutant forms of acid alpha-glucosidase. Hum Mutat. 2009;30(12):1683–1692.

9. Porto C, Ferrara MC, Meli M, Acampora E, Avolio V, Rosa M, Cobucci-Ponzano B, Colombo G, Moracci M, Andria G, et al. Pharmacological enhancement of alpha-glucosidase by the allosteric chaperone N-acetylcysteine. Mol Ther. 2012;20(12):2201–2211.

10. Tarallo A, Damiano C, Strollo S, Minopoli N, Indrieri A, Polishchuk E, Zappa F, Nusco E, Fecarotta S, Porto C, et al. Correction of oxidative stress enhances enzyme replacement therapy in Pompe disease. EMBO Mol Med. 2021;13(11):e14434.

11. Iacono R, Minopoli N, Ferrara MC, Tarallo A, Damiano C, Porto C, Strollo S, Roig-Zamboni V, Peluso G, Sulzenbacher G, et al. Carnitine is a pharmacological allosteric chaperone of the hu-man lysosomal alpha-glucosidase. J Enzyme Inhib Med Chem. 2021;36(1):2068–2079.

12. Ng PC, Henikoff S. SIFT: predicting amino acid changes that affect protein function. Nucleic Acids Res. 2003;31(13):3812–3814.

13. Siepel A, Bejerano G, Pedersen JS, Hinrichs AS, Hou M, Rosenbloom K, Clawson H, Spieth J, Hillier LW, Richards S, et al. Evolutionarily conserved elements in vertebrate, insect, worm, and yeast genomes. Genome Res. 2005;15(8):1034–1050.

14. Stone EA, Sidow A. Physicochemical constraint violation by missense substitutions mediates impairment of protein func-tion and disease severity. Genome Res. 2005;15(7):978–986.

15. Tavtigian SV, Deffenbaugh AM, Yin L, Judkins T, Scholl T, Samollow PB, de Silva D, Zharkikh A, Thomas A. Comprehensive statistical study of 452 BRCA1 missense substitutions with classification of eight recurrent substitutions as neutral. J Med Genet. 2006;43(4):295–305.

16. Davydov EV, Goode DL, Sirota M, Cooper GM, Sidow A, Batzoglou S. Identifying a high fraction of the human ge-nome to be under selective constraint using GERP++. PLoS Comput Biol. 2010;6(12):e1001025.

17. Pollard KS, Hubisz MJ, Rosenbloom KR, Siepel A. Detection of nonneutral substitution rates on mammalian phylogenies. Genome Res. 2010;20(1):110–121.

18. Reva B, Antipin Y, Sander C. Predicting the functional impact of protein mutations: application to cancer genomics. Nucleic Acids Res. 2011;39(17):e118.

19. Choi Y, Sims GE, Murphy S, Miller JR, Chan AP. Predicting the functional effect of amino acid substitutions and indels. PLOS One. 2012;7(10):e46688.

20. Shihab HA, Gough J, Cooper DN, Stenson PD, Barker GL, Edwards KJ, Day IN, Gaunt TR. Predicting the functional, mo-lecular, and phenotypic consequences of amino acid substi-tutions using hidden Markov models. Hum Mutat. 2013;34(1):57–65.

21. Mi H, Muruganujan A, Huang X, Ebert D, Mills C, Guo X, Thomas PD. Protocol update for large-scale genome and gene function analysis with the PANTHER classification sys-tem (v.14.0). Nat Protoc. 2019;14(3):703–721.

22. Garcia FAO, de Andrade ES, Palmero EI. Insights on variant analysis in silico tools for pathogenicity prediction. Front Genet. 2022;13:1010327.

23. Yamamoto K, Davis BG. Creation of an alpha-mannosynthase from a broad glycosidase scaffold. Angew Chem Int Ed Engl. 2012;51(30):7449–7453.

24. Ernst HA, Lo Leggio L, Willemoës M, Leonard G, Blum P, Larsen S. Structure of the Sulfolobus solfataricus alpha-glucosidase: implications for domain conservation and substrate recognition in GH31. J Mol Biol. 2006;358(4):1106–1124.

25. Drula E, Garron ML, Dogan S, Lombard V, Henrissat B, Terrapon N. The carbohydrate-active enzyme database: func-tions and literature. Nucleic Acids Res. 2022;50(D1):D571–D577.

26. Arumapperuma T, Li J, Hornung B, Soler NM, Goddard-Borger ED, Terrapon N, Williams SJ. A subfamily classification to cho-reograph the diverse activities within glycoside hydrolase family 31. J Biol Chem. 2023;299(4):103038.

27. Lombard V, Henrissat B, Garron ML. CAZac: an activity de-scriptor for carbohydrate-active enzymes. Nucleic Acids Res. 2025;53(D1):D625–D633.

28. Rolfsmeier M, Blum P. Purification and characterization of a maltase from the extremely thermophilic crenarchaeote Sulfolobus solfataricus. J Bacteriol. 1995;177(2):482–485.

29. Rolfsmeier M, Haseltine C, Bini E, Clark A, Blum P. Molecular characterization of the alpha-glucosidase gene (malA) from the hyperthermophilic archaeon Sulfolobus solfataricus. J Bacteriol. 1998;180(5):1287–1295.

30. Reuser AJJ, van der Ploeg AT, Chien YH, Llerena JJr., Abbott MA, Clemens PR, Kimonis VE, Leslie N, Maruti SS, Sanson BJ, et al. GAA variants and phenotypes among 1,079 patients with Pompe disease: data from the Pompe Registry. Hum Mutat. 2019;40(11):2146–2164.

31. Roig-Zamboni V, Cobucci-Ponzano B, Iacono R, Ferrara MC, Germany S, Bourne Y, Parenti G, Moracci M, Sulzenbacher G. Structure of human lysosomal acid alpha-glucosidase—a guide for the treatment of Pompe disease. Nat Commun. 2017;8(1):1111.

32. Blair HA. Cipaglucosidase alfa: first approval. Drugs. 2023;83(8):739–745.

33. Parenti G, Andria G, Valenzano KJ. Pharmacological chaper-one therapy: preclinical development, clinical translation, and prospects for the treatment of lysosomal storage disorders. Mol Ther. 2015;23(7):1138–1148.

34. D'Alonzo D, De Fenza M, Porto C, Iacono R, Huebecker M, Cobucci-Ponzano B, Priestman DA, Platt F, Parenti G, Moracci M, et al. N-Butyl-L-deoxynojirimycin (L-NBDNJ): synthesis of an allosteric enhancer of alpha-glucosidase activity for the treatment of Pompe disease. J Med Chem. 2017;60(23):9462–9469.

35. Keyzor I, Shohet S, Castelli J, Sitaraman S, Veleva-Rotse B, Weimer JM, Fox B, Willer T, Tuske S, Crathorne L, et al. Therapeutic role of pharmacological chaperones in lysosomal storage disorders: a review of the evidence and informed ap-proach to reclassification. Biomolecules. 2023;13(8):1227.

36. Bellotti AS, Andreoli L, Ronchi D, Bresolin N, Comi GP, Corti S. Molecular approaches for the treatment of Pompe disease. Mol Neurobiol. 2020;57(2):1259–1280.

37. Kok K, Kuo CL, Katzy RE, Lelieveld LT, Wu L, Roig-Zamboni V, van der Marel GA, Codee JDC, Sulzenbacher G, Davies GJ, et al. 1,6-epi-Cyclophellitol cyclosulfamidate is a bona fide lysosomal alpha-glucosidase stabilizer for the treatment of Pompe disease. J Am Chem Soc. 2022;144(32):14819–14827.

38. Sievers F, Higgins DG. Clustal Omega for making accurate alignments of many protein sequences. Protein Sci. 2018;27(1):135–145.

39. Bradford MM. A rapid and sensitive method for the quantitation of microgram quantities of protein utilizing the principle of protein–dye binding. Anal Biochem. 1976;72(1–2): 248–254.

40. Niesen FH, Berglund H, Vedadi M. The use of differential scanning fluorimetry to detect ligand interactions that promote protein stability. Nat Protoc. 2007;2(9):2212–2221.